Ab Initio Study of the Hydration of CO_2 by Carbonic Anhydrase. A Comparison between the Lipscomb and Lindskog Mechanisms†

Miquel Solà, Agustí Lledós, Miquel Duran, and Juan Bertrán*

Contribution from the Departament de Química, Universitat Autònoma de Barcelona, 08193 Bellaterra, Catalonia, Spain. *Received May 31, 1991*

Abstract: The binding of CO_2 to the biochemically active species $EZn^{II}(OH^-)$ and the generation of the EZn^{II}-bound HCO_3^- species via the Lipscomb and Lindskog mechanisms have been studied through ab initio calculations. It has been found that both mechanisms can be invoked to explain experimental data. Our results indicate that inclusions of environmental effects in the reaction coordinate are important in both mechanisms and are especially relevant in the case of the Lipscomb mechanism.

Introduction

The field of computational chemistry has experienced important advances in the last decade. Nowadays it is possible for chemists to study theoretically a complex system such as a biochemical catalyst. Moreover, theoretical studies can be merged with experimental data toward a final understanding of enzymatic reaction mechanisms. One of the subjects where computational chemistry has lately shed more light has been the study of carbonic anhydrase (CA), which is a zinc metalloenzyme that catalyzes the reversible hydration of CO_2 to yield bicarbonate anion with extreme efficiency.[1-7] X-ray data[8-11] show that the zinc atom placed at the active site of CA is bound to three imidazole groups coming from His94, His96, and His119, whereas a water molecule completes a nearly symmetrical tetrahedral coordination geometry. The hydroxyl of Thr199 is hydrogen-bound via its oxygen to the zinc-bound water and via its hydroxyl hydrogen to Glu106. The enzyme site can be divided into hydrophilic and hydrophobic halves. The hydrophilic half contains the proton acceptor group His64 and partially ordered water molecules. The inner water environment is almost completely separated from the outer channel by a ring of residues including His64, His67, Phe91, Glu92, and His200. Therefore, the inner water molecules are not in contact with those which are outside the active site. His64 bridges these two solvent areas. In the hydrophobic half, a "deep" water molecule, which is thought to be displaced by CO_2 during substrate binding, is found about 3.2 Å away from the zinc ion.

It is almost universally accepted that a zinc-bound hydroxide ion is the nucleophile in this catalytic reaction.[3-7,12] A simplified model for its mechanism involves the following four steps:[4] (1) proton transfer from $EZn^{II}(OH_2)$ in order to generate the catalytic species $EZn^{II}(OH^-)$; (2) binding of CO_2 near the active species $EZn^{II}(OH^-)$; (3) generation of the EZn^{II}-bound HCO_3^- species; and (4) binding of a water molecule and release of HCO_3^-. Different experimental studies[13-17] have shown the first step to be rate-limiting at high buffer concentrations. Given that the maximal turnover of human carbonic anhydrase II (HCAII) is measured to be 10^6 s^{-1}, the energy barrier for this intramolecular proton transfer must be about 10 kcal/mol.[18]

In spite of a general agreement with the four steps enumerated above, there is great controversy about the mechanism of the formation of EZn^{II}-bound HCO_3^-. As yet, two mechanisms have been proposed for step 3, namely, the Lipscomb and Lindskog mechanisms (see Scheme I). In the first one, following the nucleophilic attack of the $EZn(OH^-)$ group to the CO_2 molecule, there is a proton transfer between two oxygens,[19] whereas in the second mechanism there is no proton transfer but rather the oxygen atom which becomes directly coordinated to Zn^{2+} changes.[20] As a support to the Lipscomb mechanism, experiment shows[21] that when the hydrogen of HCO_3^- is substituted by an alkyl group (R), the resulting alkyl carbonate anions ($ROCO_2^-$) exhibit no substrate activities in the enzyme-catalyzed reaction. If steric and pK_a factors are not problems, this result may support the proton

Scheme I

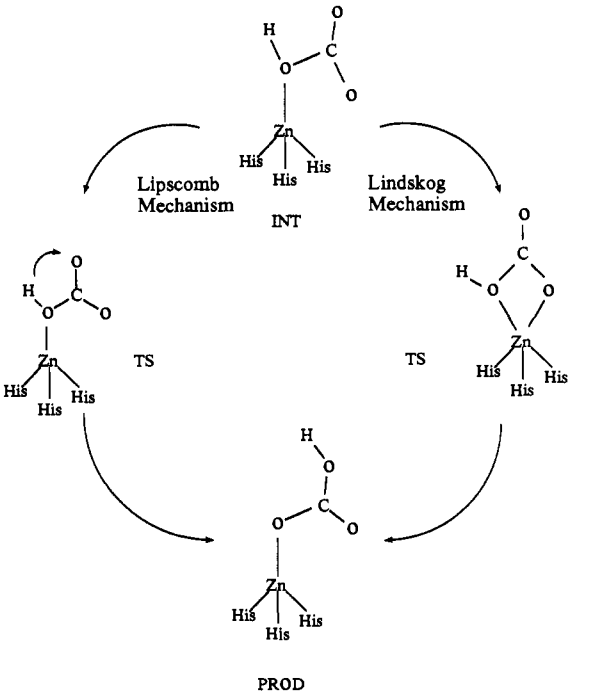

† Contribution from the "Grup de Química Quântica de l'Institut d'Estudis Catalans".

(1) Prince, R. H.; Woolley, P. R. *J. Chem. Soc., Dalton Trans.* **1972**, 1548.
(2) Williams, T. J.; Henkens, R. W. *Biochemistry* **1985**, *24*, 2459.
(3) Sen, A. C.; Tu, C. K.; Thomas, H.; Wynns, G. C.; Silverman, D. N. In *Zinc Enzymes*; Bertini, I., Luchinat, C., Maret, W., Zeppezauer, M., Eds.; Birkhäuser: Boston, 1986; Vol. I, p 329.
(4) Silverman, D. N.; Lindskog, S. *Acc. Chem. Res.* **1988**, *21*, 30.
(5) Woolley, P. *Nature* **1975**, *258*, 677.
(6) Bertini, I.; Luchinat, C. *Acc. Chem. Res.* **1983**, *16*, 272.
(7) Pocker, Y.; Deits, T. L. *J. Am. Chem. Soc.* **1982**, *104*, 2424.
(8) Kannan, K. K.; Petef, M.; Fridborg, K.; Lövgren, S.; Ohlsson, A.; Petef, M. *Proc. Natl. Acad. Sci. U.S.A.* **1975**, *72*, 51.
(9) Kannan, K. K.; Petef, M.; Fridborg, K.; Cid-Dresdner, H.; Lövgren, S. *FEBS Lett.* **1977**, *73*, 115.
(10) Liljas, A.; Kannan, K. K.; Bergsten, P.-C.; Waara, I.; Fridborg, K.; Strandberg, B.; Carlbom, U.; Järup, L.; Lövgren, S.; Petef, M. *Nature New Biol.* **1972**, *235*, 131.
(11) Eriksson, E. A.; Jones, T. A.; Liljas, A. In *Zinc Enzymes*; Bertini, I., Luchinat, C., Maret, W., Zeppezauer, M., Eds.; Birkhäuser: Boston, 1986; Vol. I, p 317.
(12) Davis, R. P. *J. Am. Chem. Soc.* **1959**, *81*, 5674.
(13) Pocker, Y.; Janjić, N. *J. Am. Chem. Soc.* **1989**, *111*, 731.
(14) Silverman, D. N.; Tu, C. K. *J. Am. Chem. Soc.* **1975**, *97*, 2263.
(15) Coates, J. H.; Gentle, G. J.; Lincoln, S. F. *Nature* **1974**, *249*, 773.
(16) Pocker, Y.; Miao, C. H. *Biochemistry* **1987**, *26*, 8481.
(17) Steiner, H.; Jonsson, B.-H.; Lindskog, S. *Eur. J. Biochem.* **1975**, *59*, 253.
(18) Merz, K. M., Jr.; Hoffmann, R.; Dewar, M. J. S. *J. Am. Chem. Soc.* **1989**, *111*, 5636.

0002-7863/92/1514-869$03.00/0

transfer. ^{13}C NMR[4,22] and proton-inventory[17] experiments favor the Lindskog mechanism, showing that there is no rate-limiting proton transfer during the CO_2/HCO_3^- interconversion.

Recently, three leading theoretical groups have studied the hydration of CO_2 catalyzed by CA. Their results, which are not coincident, have not clarified the controversy yet. Liang and Lipscomb,[23-25] using the PRDDO method, showed that the Lipscomb mechanism is favored over the Lindskog mechanism because the energy barrier for the internal proton transfer is much lower when appropriate proton relay is considered. Merz, Hoffmann, and Dewar[18] used the AM1 method to perform an exhaustive analysis of the different steps of the CA mechanism. These authors presented the transition state corresponding to the Lindskog mechanism with a calculated energy barrier of 13.1 kcal/mol. Nonetheless, they were unable to locate a transition state for the Lipscomb mechanism, so the comparison between the two mechanisms was not performed. Finally, Jacob, Cardenas, and Tapia[26] carried out ab initio calculations with an extended basis set, finding that the transition state for the Lindskog mechanism is 50 kcal/mol more stable at the SCF level than for the Lipscomb mechanism. This difference in energy barriers decreases by 20 kcal/mol if correlation energy is taken into account.

The main problem found in theoretical biochemistry is how to model enzymatic reactions.[27] In the case of CA, the short description of the active site given above evidences its complexity and, hence, the difficulty of its modeling. This great complexity forces introduction of important simplifications in order to perform calculations. Different approaches have been suggested depending on the problem studied. For instance, molecular mechanics,[28-30] semiempirical,[18,23-25] ab initio,[26,31-35] free energy simulations,[36,37] and molecular dynamics[38] methods have been used at several levels of sophistication and applied to different models of the active site.

The main goal of our work is to compare the two mechanisms proposed for step 3 of the CA catalytic cycle. Since our purpose is to obtain reliable structures for transition states and meaningful energy barriers for these two mechanisms, an ab initio methodology is used. However, the size of the system studied is quite large, so we are forced to simplify the theoretical description of the active site by excluding all proteinic residues and, in a first step, all water molecules. The simplest model for the active site is a Zn^{II}-bound hydroxide species; however, this is not really a good choice: charge transfer from the ligands translates into an $EZn^{II}(OH^-)$ species which is more nucleophilic than the $Zn^{II}(OH^-)$ complex,[32] so use of Zn^{II}-bound hydroxide as a model for the enzyme makes a correct analysis of the process difficult. Therefore, a less simplified model would involve ligands coordinated to Zn^{2+} which should be incorporated in the model of the active site. Moreover, previous theoretical studies have stressed the importance of considering additional water molecules in some proton-transfer processes.[39-51] These water molecules facilitate the proton relay by acting as bifunctional catalysts. Because in the Lipscomb mechanism there is a proton transfer between two oxygens, we should introduce additional water molecules in our model when studying this mechanism. Finally, there is one problem left: modeling the remaining groups still present at the active site, both the proteinic residues and water molecules. One can expect that the electric field created by this environment may modify the energy barriers.[52-55] So this effect should be considered for a good description of the enzymatic reaction. Because the use of an ab initio methodology impedes the specific description of each remainding residue present at the active site, it has been necessary to separate the chemical system from its environment, and to include the effect of this environment in an average way through a continuum model.

Methodology

Ab initio all-electron SCF calculations were performed by means of the Hartree–Fock–Roothaan method.[56] Correlation energy was included at the MP2 level.[57] Owing to computational limitations, three ammonia groups were used to simulate the three imidazole ligands of the zinc ion, resulting in the $(NH_3)_3Zn^{II}(OH^-)$ complex being our model of the CA active site; the validity of this substitution, which is necessary to perform ab initio calculations, is supported by previous studies of Pullman et al.[56,59] who demonstrated that ammonia and imidazole transfer a similar amount of charge to Zn^{2+}. The geometry of each NH_3 group was kept frozen with the N–H distance being 1.05 Å and the HNH angles being tetrahedral. C_{3v} symmetry was imposed on the $(NH_3)_3Zn^{II}$ fragment, except for the Lindskog transition state where this fragment had only C_s symmetry. Under the aforementioned geometric constraints, full geometry optimizations of minima and transition states (TS) were performed using Schlegel's method.[60] Minima and transition states were characterized by the correct number of negative eigenvalues of their Hessian matrices. The 3-21G basis set[61,62] was used for all atoms but for hy-

(19) Lipscomb, W. N. *Annu. Rev. Biochem.* **1983**, *52*, 17.
(20) Lindskog, S. In *Zinc Enzymes*; Spiro, T. G., Ed.; Wiley: New York, 1983; p 77.
(21) Pocker, Y.; Deits, T. L. *J. Am. Chem. Soc.* **1983**, *105*, 980.
(22) Simonsson, I.; Jonsson, B.-H.; Lindskog, S. *Eur. J. Biochem.* **1979**, *93*, 409.
(23) Liang, J.-Y.; Lipscomb, W. N. *Biochemistry* **1987**, *26*, 5293.
(24) Liang, J.-Y.; Lipscomb, W. N. *Biochemistry* **1988**, *27*, 8676.
(25) Liang, J.-Y.; Lipscomb, W. N. *Int. J. Quantum Chem.* **1989**, *36*, 299.
(26) Jacob, O.; Cardenas, R.; Tapia, O. *J. Am. Chem. Soc.* **1990**, *112*, 8692.
(27) Alagona, G.; Ghio, C. In *The Enzyme Catalysis Process*; Cooper, A., Houben, J. L., Chien, L. C., Eds.; Plenum: New York, 1989; p 345.
(28) Vedani, A.; Huhta, D. W.; Jacober, S. P. *J. Am. Chem. Soc.* **1989**, *111*, 4075.
(29) Vedani, A.; Huhta, D. W. *J. Am. Chem. Soc.* **1990**, *112*, 4759.
(30) Vedani, A. *J. Comput. Chem.* **1988**, *9*, 269.
(31) Liang, J.-Y.; Lipscomb, W. N. *Biochemistry* **1989**, *28*, 9724.
(32) Bertini, I.; Luchinat, C.; Rosi. M.; Sgamellotti, A.; Tarantelli, F. *Inorg. Chem.* **1990**, *29*, 1460.
(33) Vedani, A.; Dobler, M.; Dunitz, J. D. *J. Comput. Chem.* **1986**, *7*, 701.
(34) De Benedetti, P. G.; Menziani, M. C.; Cocchi, M.; Frassineti, G. *J. Mol. Struct. (THEOCHEM)* **1989**, *183*, 393.
(35) Pullman, A.; Demoulin, D. *Int. J. Quantum Chem.* **1979**, *16*, 641.
(36) Merz, K. M., Jr. *J. Am. Chem. Soc.* **1991**, *113*, 406.
(37) Menziani, M. C.; Reynolds, C. A.; Richards, W. G. *J. Chem. Soc., Chem. Commun.* **1989**, 853.
(38) Reynolds, J. C. L.; Cooke, K. F.; Northrup, S. H. *J. Phys. Chem.* **1990**, *94*, 985.
(39) Lledós, A.; Bertrán, J. *J. Mol. Struct. (THEOCHEM)* **1985**, *120*, 73.
(40) Lledós, A.; Bertrán, J. *J. Mol. Struct. (THEOCHEM)* **1984**, *107*, 233.
(41) Nguyen, M. T.; Ha, T.-K. *J. Am. Chem. Soc.* **1984**, *106*, 599.
(42) Lledós, A.; Bertrán, J. *Tetrahedron Lett.* **1981**, *22*, 75.
(43) Lledós, A.; Bertrán, J. *J. Mol. Struct. (THEOCHEM)* **1984**, *107*, 233.
(44) Ventura, O. N.; Lledós, A.; Bonaccorsi, R.; Bertrán, J.; Tomasi, J. *Theor. Chim. Acta* **1987**, *72*, 175.
(45) Ruelle, P.; Kesselring, U. W.; Nam-Tram, H. *J. Mol. Struct. (THEOCHEM)* **1985**, *124*, 41.
(46) Ruelle, P.; Kesselring, U. W.; Nam-Tram, H. *J. Am. Chem. Soc.* **1986**, *108*, 371.
(47) Ruelle, P. *Chem. Phys.* **1986**, *110*, 263.
(48) Ruelle, P. *J. Comput. Chem.* **1987**, *8*, 158.
(49) Ruelle, P. *J. Am. Chem. Soc.* **1987**, *109*, 1722.
(50) Nguyen, M. T.; Ruelle, P. *Chem. Phys. Lett.* **1987**, *138*, 486.
(51) Oie, T.; Loew, G. H.; Burt, S. K.; MacElroy, R. D. *J. Am. Chem. Soc.* **1983**, *105*, 2221.
(52) Bertrán, J. In *New Theoretical Concepts for Understanding Organic Reactions*; Bertrán, J., Csizmadia, I. G., Eds.; Kluwer Academic Press: New York, 1989; p 231.
(53) Andrés, J. L.; Lledós, A.; Duran, M.; Bertrán, J. *Chem. Phys. Lett.* **1988**, *153*, 82.
(54) Solà, M.; Lledós, A.; Duran, M.; Bertrán, J. *Int. J. Quantum Chem.*, in press.
(55) Solà, M.; Lledós, A.; Duran, M.; Bertrán, J.; Abboud, J. L. M. *J. Am. Chem. Soc.* **1991**, *113*, 2873.
(56) Roothaan, C. C. J. *Rev. Mod. Phys.* **1951**, *23*, 69.
(57) Møller, C.; Plesset, M. S. *Phys. Rev.* **1934**, *46*, 618.
(58) Demoulin, D.; Pullman, A. *Theor. Chim. Acta* **1978**, *49*, 161.
(59) Pullman, A. *Ann. N.Y. Acad. Sci.* **1981**, *367*, 340.
(60) Schlegel, H. B. *J. Comput. Chem.* **1982**, *3*, 214.
(61) Binkley, J. S.; Pople, J. A.; Hehre, W. J. *J. Am. Chem. Soc.* **1980**, *102*, 939.

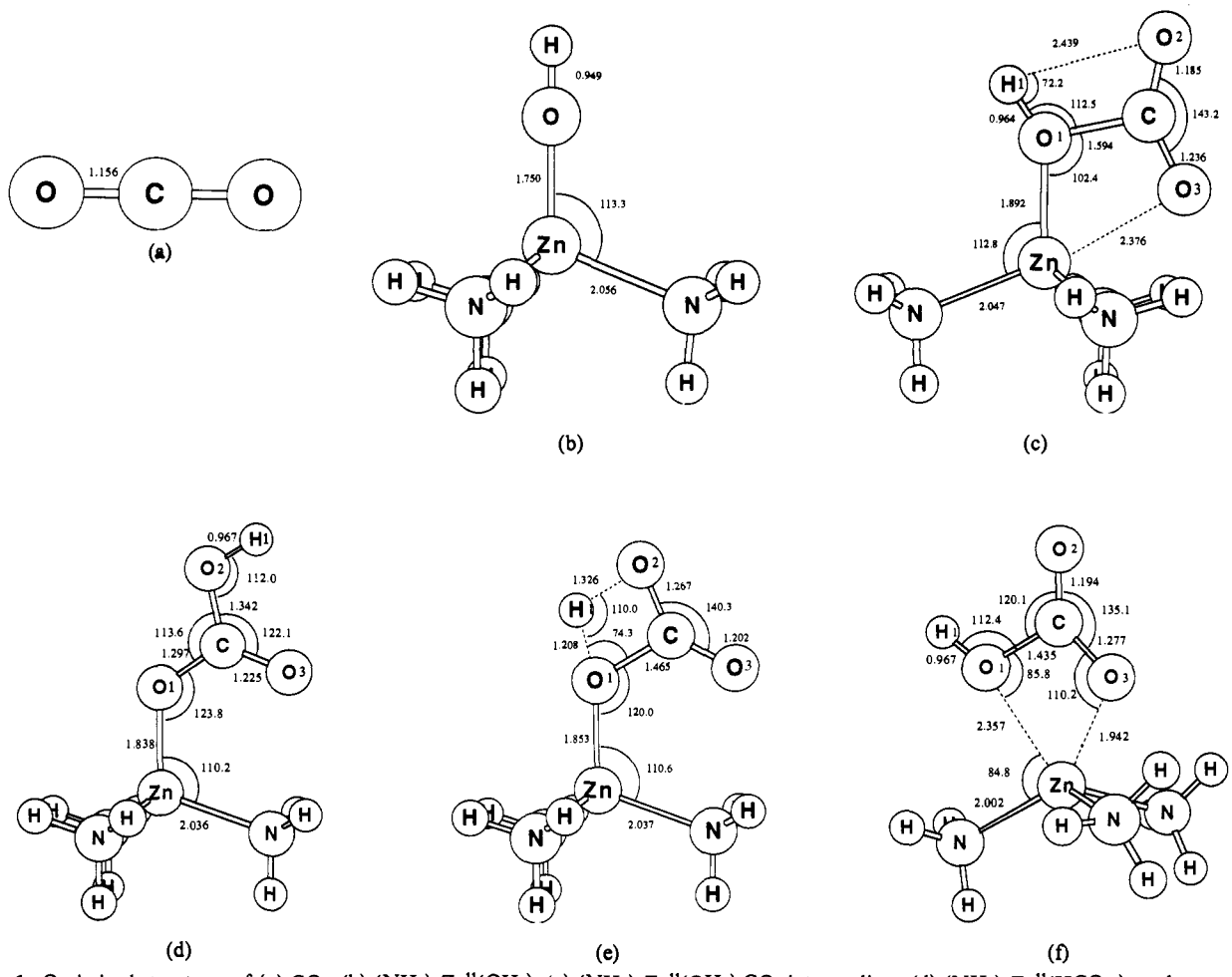

Figure 1. Optimized structures of (a) CO_2; (b) $(NH_3)_3Zn^{II}(OH^-)$; (c) $(NH_3)_3Zn^{II}(OH^-)\cdot CO_2$ intermediate; (d) $(NH_3)_3Zn^{II}(HCO_3^-)$ product anti; (e) $(NH_3)_3Zn^{II}(OH^-)\cdot CO_2$ Lipscomb TS; and $(NH_3)_3Zn^{II}(OH^-)\cdot CO_2$ Lindskog TS.

drogens of the NH_3 groups for which the STO-3G basis set[63] was used.

To introduce the environment effect, the SCRF model due to Tomasi et al.[64-66] was used. In this model the environment is represented by a continuous polarizable dielectric with permitivity ϵ, and the solute is placed inside a cavity accurately defined by its own geometry.[67] Dielectric polarization due to the solute is simulated by the creation of a system of virtual charges on the cavity surface. The charge distribution on the surface polarizes in turn the charge distribution in the solute. This process is iterated until obtaining self-consistency in the solute electron density. In this way, the feed-back effect of the environment on the solute is taken into account. The electrostatic contribution to the solvation free energy is found as the difference between the energies computed with the continuum model and without it minus one-half of the interaction energy between the charge distribution of the solute and the reaction field potential.[65] Moreover, the cavitation free energy is calculated with Pierotti's equation.[68] The geometries optimized in the gas phase (ϵ = 1.00) were used throughout.

All calculations presented in this paper were carried out with the help of the GAUSSIAN 86[69] and MONSTERGAUSS[70] programs. The surrounding medium effect was studied with a FORTRAN subroutine written by Tomasi and co-workers and incorporated in the MONSTERGAUSS program.

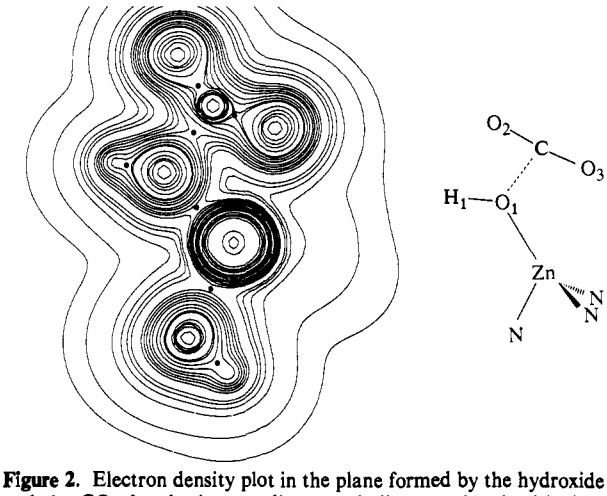

Figure 2. Electron density plot in the plane formed by the hydroxide ion and the CO_2 for the intermediate. ● indicates a bond critical point.

Results and Discussion

Presentation of the results obtained is split into two sections. In the first section, we analyze the CO_2 hydration through the $(NH_3)_3Zn^{II}(OH^-)$ model for the CA active site, whereas in the second section we discuss the effect of the surrounding medium in the reaction.

(62) Dobbs, K. D.; Hehre, W. J. *J. Comput. Chem.* **1987**, *8*, 861.
(63) Hehre, W. J.; Stewart, R. F.; Pople, J. A. *J. Chem. Phys.* **1969**, *51*, 2657.
(64) Miertuš, S.; Scrocco, E.; Tomasi, J. *Chem. Phys.* **1981**, *55*, 117.
(65) Pascual-Ahuir, J. L.; Silla, E.; Tomasi, J.; Bonaccorsi, R. *J. Comput. Chem.* **1987**, *8*, 778.
(66) Floris, F.; Tomasi, J. *J. Comput. Chem.* **1989**, *10*, 616.
(67) The sphere radii used for atoms were 20% larger than the van der Waals (or ionic) radii, (hydrogen, 1.44 Å; carbon, 1.94 Å; nitrogen, 1.80 Å; oxygen, 1.68 Å; zinc, 0.84 Å). The surrounding medium effect calculations were carried out at 298.15 K.
(68) Pierotti, R. A. *Chem. Rev.* **1976**, *76*, 717.
(69) Frisch, M. J.; Binkley, J. S.; Schlegel, H. B.; Raghavachari, K.; Melius, C. F.; Martin, R. L.; Stewart, J. J. P.; Bobrowicz, F. W.; Rohlfing, C. M.; Kahn, L. R.; Defrees, D. F.; Seeger, R.; Whiteside, R. A.; Fox, D. J.; Fleider, E. M.; Pople, J. A. Program GAUSSIAN86; Carnegie-Mellon Quantum Chemistry Publishing Unit: Pittsburgh, PA, 1984.
(70) Peterson, M. R.; Poirier, R. A. Program MONSTERGAUSS; Department of Chemistry, University of Toronto: Ontario, Canada, 1981.

Table I. Charges in Atomic Units on the Atoms or Fragments of the Optimized Intermediate, Transition States, and Product[a]

	$q_{(NH_3)_3Zn}$	q_{O_1}	q_{H_1}	q_C	q_{O_2}	q_{O_3}
$(NH_3)_3Zn^{II}(OH^-)$	1.539	−0.931	0.392			
CO_2				1.083	−0.541	−0.541
$(NH_3)_3Zn^{II}(OH^-)\cdot CO_2$	1.641	−0.842	0.447	1.132	−0.619	−0.759
$(NH_3)_3Zn^{II}(OH^-)\cdot CO_2$ Lipscomb TS	1.681	−0.906	0.500	1.148	−0.731	−0.692
$(NH_3)_3Zn^{II}(OH^-)\cdot CO_2$ Lindskog TS	1.642	−0.790	0.433	1.162	−0.823	−0.624
anti-$(NH_3)_3Zn^{II}(HCO_3^-)$	1.642	−0.835	0.424	1.188	−0.705	−0.714

[a] For atom numbering refer to Figure 1.

Hydration of CO_2 by the $(NH_3)_3Zn^{II}(OH^-)$ Model. This section is structured as follows: first, the geometries of separated reactants, intermediate, and products are presented; second, the transition-state structures for the two studied mechanisms are discussed; and third, the relative energies referred to reactants are reported together with energy barriers.

(a) Separated Reactants, Intermediate, and Products Geometries. Figure 1a–d shows the geometries of the separated reactants, intermediate, and final product. For the intermediate, the obtained value of 1.59 Å for the C–O_1 distance is similar to that reported by Lipscomb et al. (1.50 Å)[23] and that obtained by Jacob et al. (1.46 Å).[26] On the contrary, the corresponding AM1-optimized structure[18] is quite different from that presented here. In this case, the authors found that the formation of the C–O_1 bond was not initiated yet, and the Zn–O_3 bond was longer than 5 Å. Our value for the C–O_1 distance indicates that the nucleophilic attack of the Zn^{II}-bound OH^- to CO_2 is quite advanced. The density map[71] for this intermediate (Figure 2) reinforces this point, showing the existence of a bond critical point[72] between C and O_1. The deformation of the ZnO_1H_1 and O_2CO_3 angles, as compared to their values in the separated reactants, and the Mayer bond order for the C–O_1 distance (0.473) bring about the same conclusion. The values of charges (Table I) show that the charge transfer from the Zn^{II}-bound OH^- to CO_2 is 0.246 au, thus indicating again that in this intermediate the nucleophilic attack has already been produced to a great extent.

The Zn–O_1 distance evolves from 1.75 Å in the reactants to 1.89 Å in the intermediate. It is well known that the reaction between CO_2 and OH^- proceeds with no barrier in the gas phase.[73] On the contrary, in solution a barrier of 13.2 kcal/mol has been detected.[74] This barrier is originated because the charge transfer from OH^- to CO_2 carries an important desolvation of the hydroxide ion. In this reaction, the $(NH_3)_3Zn^{II}$ group plays a role similar to that of solvent molecules. As mentioned above, during the nucleophilic attack the Zn–O_1 distance increases, similar to the way solvent molecules separate from the substrate in a desolvation process. The increase in the Zn–O_1 distance is also accompanied by an increase in the OH^- nucleophilic character which facilitates the subsequent nucleophilic attack.

From the electron density map of the intermediate (Figure 2), it emerges clearly that no bond critical point between Zn and O_3 has been formed, although given the positive charge on the Zn atom and the negative charge on O_3 there is an important electrostatic interaction between Zn and O_3. Despite the absence of a direct chemical bond between Zn and O_3, from a geometrical point of view CO_2 could be considered as a fifth distant ligand, in good agreement with the results obtained by Lipscomb,[23] Pullman,[58,59] and Jacob et al.[26]

Experimental NMR ^{13}C work has shown in a Cu(II)-substituted CA that the Cu–C distance is 3.2 Å.[75] Despite the fact that Cu(II)-substituted CA is an inactive species, for the Co(II)-substituted CA which retains about 55% of the activity of the wild type, similar results are reported.[76] Recent molecular dynamics and free-energy perturbation simulations results[36] have identified the presence of two CO_2 binding sites. One of them has a Zn–C distance of 3–4 Å; its calculated binding energy of −3.4 kcal/mol is also in reasonable agreement with the experimental value of −2.2 kcal/mol.[77] In our intermediate, the Zn–C distance is 2.72 Å, which is too short to account for the experimental values. This is a first indication that our intermediate does not correspond exactly to the observed experimental structure (where the interaction of CO_2 with the proteinic residues at the active site may be essential), but rather our intermediate corresponds to a subsequent stage of the interaction where the nucleophilic attack has been already initiated.

The most relevant fact in this stage of the reaction is the polarization of the CO_2 fragment induced by the Zn^{II}-bound hydroxide species. This polarization appears despite a charge transfer from this group to CO_2. Table I shows that the C atom increases its positive charge by 0.049 electron, and that the difference between the O_3 and O_2 negative charges becomes 0.140 electron. The increased negative charge on the O_3 atom accounts for the important electrostatic interaction between Zn and O_3. Further, the increase in the positive charge on the C atom favors the later nucleophilic attack of the O_1 atom to C. This CO_2 activation, due to the presence of the Zn^{2+} dication, has been previously emphasized,[18,23,35] especially in the article of Jacob et al.[26]

The final product of the reaction is shown in Figure 1d. The product exhibits two possible conformations, depending on whether H_1 is closer to O_1 than to O_3 (this product hereafter named syn-) or, in contrast, H_1 is closer to O_3 than to O_1 (this product hereafter named anti-). The latter turns out to be the most stable, although the slight differences between these two structures may result in a fast interconversion rate between them.

(b) Transition-State Geometries. As mentioned in the Introduction, two mechanisms have been proposed to date for the formation of the HCO_3^- anion in the CA enzyme, namely, the Lipscomb and Lindskog mechanisms.

In this study we have been able to locate the transition states corresponding to both mechanisms; we have also checked that both transition states connect the intermediate with the product described above.

In Figure 1e the transition state found for Lipscomb mechanism, which involves a proton transfer between two oxygens, is depicted. The four atoms involved most in the process (O_1, H_1, O_2, and C) form a four-membered ring. The distances are similar to those found by Liang and Lipscomb[23] using the PRDDO method. The largest differences appear in the O_1–H_1 and O_2–H_1 distances (1.113 and 1.554 Å, respectively, with the PRDDO method), showing that in the present study the proton transfer in the transition state is more advanced than the PRDDO results predict. Furthermore, the C–O_1 distance (1.524 Å with the PRDDO method) shows that the nucleophilic attack is a little more advanced in the present case. The distance between Zn and O_3 increases in the transition state, so the metal coordination remains unchanged. This point is stressed by the electron density map of the transition state (Figure 3) where no bond critical point between Zn and O_3 appears. Another remarkable fact in this map turns out to be the presence of a ring critical point, showing that

(71) The lines plotted in all the electron isodensity maps presented in this work correspond to the values of 0.0001, 0.001, 0.01, 0.02, 0.03, 0.04, 0.08, 0.1, 0.12, 0.15, 0.18, 0.24, 0.3, 0.37, 0.40, 0.60, 0.80, 1.0, 1.5, 10, and 100 au.

(72) Bader, R. F. W. *Acc. Chem. Res.* **1985**, *18*, 9.
(73) Jönsson, B.; Karlström, G.; Wennerström, H. *J. Am. Chem. Soc.* **1978**, *100*, 1658.
(74) Pinsent, B. R. W.; Pearson, L.; Roughton, F. J. W. *Trans. Faraday Soc.* **1956**, *52*, 1512.
(75) Bertini, I.; Borghi, E.; Luchinat, C. *J. Am. Chem. Soc.* **1979**, *101*, 7069.
(76) (a) Prince, R. H.; Woolley, P. R. *Angew. Chem., Int. Ed. Engl.* **1972**, *11*, 408. (b) Henkens, R. W.; Merrill, S. P.; Williams, T. J. In *Biology and Chemistry of the Carbonic Anhydrases*; Tashian, R. E., Hewett-Emmett, D., Eds.; *Ann. New York Acad. Sci.* **1984**, *429*, 143.
(77) Led, J. J.; Neesgaard, E. *Biochemistry* **1987**, *26*, 183.

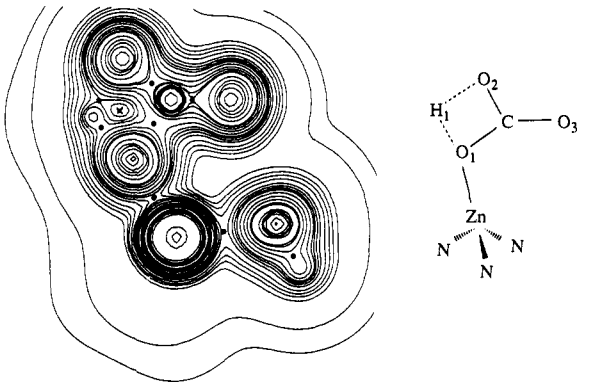

Figure 3. Electron density plot in the plane formed by the hydroxide ion and the CO_2 for the transition state which corresponds to the Lipscomb mechanism. ● indicates a bond critical point, while × indicates a ring critical point.

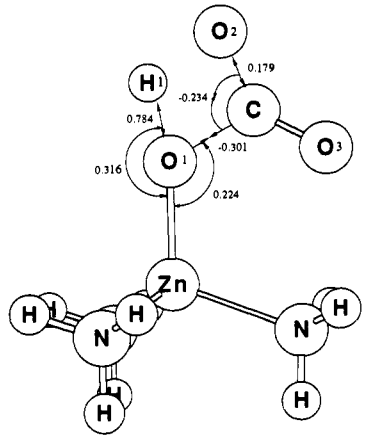

Figure 4. Main components of the transition vector (in internal coordinates) corresponding to the Lipscomb mechanism.

a four-membered ring between H_1, O_1, O_2, and C has been indeed formed.

To get a deeper insight into this mechanism, the main components of the transition vector (in internal coordinates) are drawn in Figure 4. One can see that the nucleophilic attack and the proton transfer are concerted processes; however, these two processes are not advanced to the same extent. Whereas the nucleophilic attack is almost completed in the transition state, the proton is only half-way transferred. The largest components of the transition vector correspond to this proton transfer, even though there is an important component corresponding to the nucleophilic attack (-0.30). In any case, the transfer of H_1 from O_1 to O_2 will account for the largest part of the energy barrier.

The transition state found for the Lindskog mechanism, which bears a change of the oxygen directly coordinated to Zn^{2+}, is depicted in Figure 1f. In this transition state, the Zn–O_1 bond is almost broken and the Zn–O_3 bond is almost formed. Further, the Mayer bond orders for these two bonds are 0.190 and 0.473, respectively. The electron density map (Figure 5) shows that no ring critical point between Zn, O_1, C, and O_3 has been formed, and that the Zn–O_1 bond is already broken whereas the Zn–O_3 bond is almost completely formed. In this transition state the interaction between Zn and O_1 is merely electrostatic. The main components of the transition vector in internal coordinates (Figure 6) bring about the same conclusions: breaking of the Zn–O_1 bond together with the formation of a new Zn–O_3 bond. The O_1–H_1 distance remains unchanged, and participation of H_1 in the transition vector is due merely to spatial reorientation of the O_1–H_1 bond.

(c) Energetics. Table II collects the energies of the different structures mentioned above, referred to separated reactants, and the forward and backward energy barriers for the Lipscomb and Lindskog mechanisms.

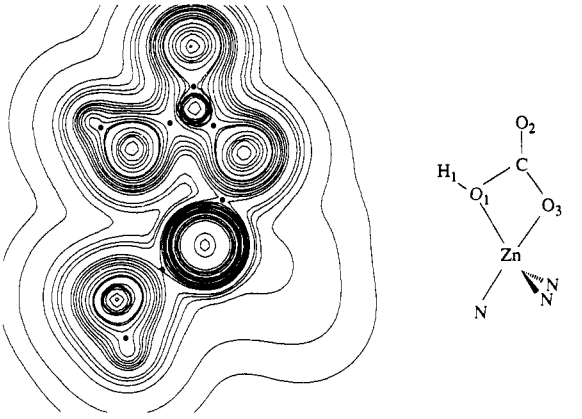

Figure 5. Electron density plot in the plane formed by the hydroxide ion and the CO_2 for the transition state which corresponds to the Lindskog mechanism. ● indicates a bond critical point.

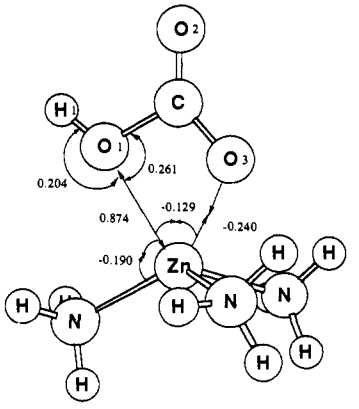

Figure 6. Main components of the transition vector (in internal coordinates) corresponding to the Lindskog mechanism.

Table II. Relative Energies (in kcal/mol) Referred to Separated Reactants for the Different Species Which Intervene in the CO_2 Hydration by CA in the Lipscomb and Lindskog Mechanisms, Together with Forward and Backward Energy Barriers for These Two Mechanisms, Obtained with the 3-21G Basis Set at the SCF and MP2 Levels

	SCF	MP2
$(NH_3)_3Zn^{II}(OH^-) + CO_2$	0.	0.
$(NH_3)_3Zn^{II}(OH^-)\cdot CO_2$ INT	-20.3	-12.4
$(NH_3)_3Zn^{II}(OH^-)\cdot CO_2$ Lipscomb TS	22.3	24.0
$(NH_3)_3Zn^{II}(OH^-)\cdot CO_2$ Lindskog TS	-18.1	-4.4
$(NH_3)_3Zn^{II}(HCO_3^-)$	-31.6	-15.1
forward Lipscomb	42.6	36.4
backward Lipscomb	53.9	39.1
forward Lindskog	2.2	8.0
backward Lindskog	13.5	10.7

The binding energy of CO_2 to $(NH_3)_3Zn^{II}(OH^-)$ in the intermediate complex is -20.3 kcal/mol. Pullman et al.,[58] using a very simplified electrostatic approximation, reported -8.6 kcal/mol for this interaction. On the other hand, in a recent work Jacob et al.[26] gave a value of -35.1 kcal/mol for a similar complex. All these values differ substantially from the -2.2 kcal/mol experimental binding energy;[36,77] as mentioned above, the experimental structure is an intermediate which appears earlier along the reaction coordinate. Our intermediate represents a more advanced structure in which the nucleophilic attack has been already initiated.

The computed forward and backward barriers for the Lipscomb mechanism are 42.6 and 53.9 kcal/mol. These values compare quite well with the 37.5 and 56.6 kcal/mol obtained by Liang and Lipscomb with the PRDDO method.[23] For the Lindskog mechanism, the forward and backward barriers turn out to be 2.2 and 13.5 kcal/mol. For the forward reaction Jacob et al.[26] reported an energy barrier of 2.7 kcal/mol which is not far from our

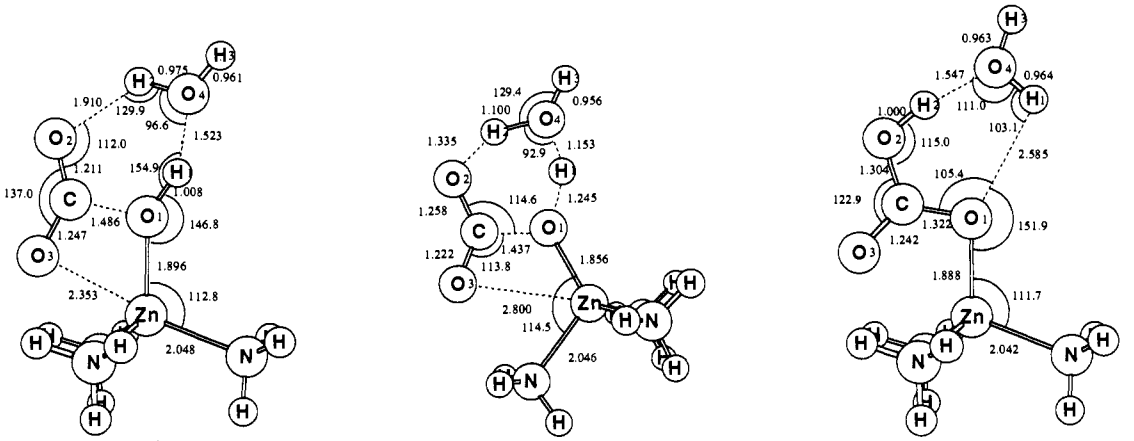

Figure 7. Optimized structures of (a) $(NH_3)_3Zn^{II}(OH^-)(CO_2)\cdot H_2O$ intermediate; (b) $(NH_3)_3Zn^{II}(OH^-)(CO_2)\cdot H_2O$ Lipscomb TS; (c) $(NH_3)_3Zn^{II}(HCO_3^-)\cdot H_2O$ product, when one additional water molecule has been considered for the proton release.

computed value. It is clearly seen that for both the forward and backward reactions the Lindskog mechanism is far more favored at the SCF level.

The final product of this CO_2 hydration reaction is 11.3 kcal/mol more stable than the intermediate complex. This fact leads to sizable differences between forward and backward energy barriers, which do not favor the necessary reversibility of all enzymatic processes. As the SCF level can overestimate the stabilization of some structures, the correlation energy at MP2 level without any reoptimization of the geometries obtained at SCF level (i.e., MP2/3-21G//3-21G) has been included.

Introduction of correlation energy at this level gives (Table II) an intermediate, a Lindskog transition state, and especially a product, which are less stabilized than separated reactants or the Lipscomb transition state. Therefore, energy barriers for the forward and backward reactions become more similar, favoring the necessary reversibility of the process, diminishing the energy barriers for the Lipscomb mechanism, and increasing the forward energy barrier for the Lindskog mechanism. Nevertheless, the Lindskog mechanism continues to be favored. As long as CO_2 hydration is not the rate-determining step in the CA catalytic cycle, the energy barrier for the CO_2 hydration must be lower than 10 kcal/mol. Therefore, results of Table II indicate that the Lipscomb mechanism would not seem to be in agreement with the present study made with this simplified model.

Environmental Effects. In this section the effect of the environment in the reaction is discussed. First, we analyze the changes produced when considering an additional discrete water molecule in our model for the active site; second, the effect of the remaining proteinic residues and water molecules is included through a continuum model.

(a) Incorporation of an Additional Water Molecule to the Description of the Active Site. So far we have used the $(NH_3)_3Zn^{II}(OH^-)$ complex as a model for the CA active site. It is well known that in the active site there is a number of water molecules, some of which could participate directly in the reaction. AM1 calculations by Merz et al.[18] show that inclusion of an additional water molecule in the model for the study of Lindskog mechanism increases the energy barrier by only 2 kcal/mol. Thus, the study of the Lindskog mechanism with an additional water molecule does not seems to be essential and will not be performed here. For the Lipscomb mechanism, the situation is quite different because it involves a proton transfer between two oxygen atoms. As commented in the Introduction, the presence of water molecules intervening directly in the proton transfer can facilitate the process by acting as bifunctional catalysts.[39-51] In fact, PRDDO calculations by Lipscomb[23,25] have shown that the barrier of 35.6 kcal/mol for a direct internal proton transfer in isolated HCO_3^- is reduced to 3.5 kcal/mol when one water molecule is included for proton release. Merz,[78] following previous work by Nguyen et al.,[41] has also found that the activation energy for the reaction of CO_2 with one water molecule is 54.5 kcal/mol, whereas for two water molecules reacting with CO_2 it is 32.3 kcal/mol. These results show that presence of water molecules may be very important in the study of the Lipscomb mechanism. For this reason, the study of this mechanism with an additional water molecule is carried out in the present paper.

Figure 7a depicts the optimized structure obtained for the intermediate when an additional water molecule is included in the description of the active site. In this structure, the incorporated water molecule forms two hydrogen bonds: O_2–H_2 and O_4–H_1. The latter bond is the strongest one, as can be seen from the O_2–H_2 and O_4–H_1 distances, and from the Mayer bond orders (0.081 and 0.176, respectively). In this intermediate, as compared to the intermediate which does not incorporate an additional water molecule, the C–O_1 distance has been reduced from 1.59 to 1.49 Å, its Mayer bond order being now 0.610. This result shows that the nucleophilic attack is now more advanced owing to the increase of the positive charge on the C atom and the negative charge on the O_1 atom induced by the two hydrogen bonds formed. The charge transfer to CO_2 is 0.324 electron in this stage of the interaction. The value of the Zn–O_3 distance has barely changed, leading to the conclusion that the CO_2 molecule continues not to be directly coordinated to Zn^{2+}.

In Figure 7b the transition state for the Lipscomb mechanism of HCO_3^- formation with an additional water molecule is depicted. Interestingly, the six atoms involved most in the process (O_1, H_1, O_4, H_4, O_2, and C) form a fairly regular six-membered ring, which is less strained than the four-membered ring found previously, and hence this transition state is stabilized. The O–H distances show that H_1 has been transferred to the water molecule, whereas this water has only begun to transfer its H_2 atom to O_2. The Mayer bond orders confirm this impression, given that the O_1–H_1, O_4–H_1, and O_4–H_2, and O_2–H_2 bond orders are 0.302, 0.376, 0.431, and 0.271, respectively. When going from the intermediate to the transition state, the C–O_1 distance changes only from 1.49 to 1.44 Å, its Mayer bond order being then 0.713. The component of the C–O_1 bond in the transition vector (Figure 8) diminishes when an additional water molecule is taken into account, being now only –0.18, thus showing that the nucleophilic attack is almost finished at this transition state. The largest components of the transition vector correspond to the motion of the H_1 and H_2 atoms in the two proton-transfer processes. In conclusion, the additional water molecule plays an active role in the reaction, as pointed out by different authors in similar processes.[39-51] The geometry of the product is given in Figure 7c. In this structure two hydrogen bonds of different intensity are also formed.

Table III contains the relative energies at the SCF and MP2 levels referred to separated reactants for the different species involved in the process, together with the values obtained for the forward and backward energy barriers for the Lipscomb mechanism when studied with an additional water molecule.

The interaction energy of a water molecule with the $(NH_3)_3Zn^{II}(OH^-)\cdot CO_2$ complex is –27.6 kcal/mol, which corresponds

(78) Merz, K. M., Jr. *J. Am. Chem. Soc.* **1990**, *112*, 7973.

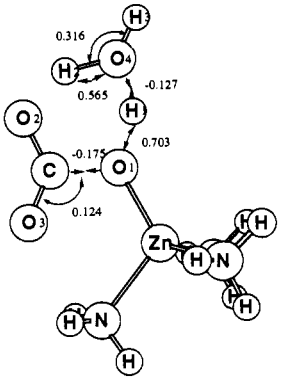

Figure 8. Main components of the transition vector (in internal coordinates) corresponding to the Lipscomb mechanism when one additional water molecule has been included in the description of the active site.

Table III. Relative Energies (in kcal/mol) Referred to Separated Reactants for the Different Species Which Intervene in the CO_2 Hydration by CA in the Lipscomb Mechanism When an Additional Water Molecule Has Been Considered in the Proton Release, Together with Forward and Backward Energy Barriers for This Mechanism, Obtained with the 3-21G Basis Set at the SCF and MP2 Levels

	SCF	MP2
$(NH_3)_3Zn^{II}(OH^-)\cdot CO_2 + H_2O$	0.	0.
$(NH_3)_3Zn^{II}(OH^-)(CO_2)\cdot H_2O$ INT	−27.6	−27.5
$(NH_3)_3Zn^{II}(OH^-)(CO_2)\cdot H_2O$ TS	−8.5	−10.5
$(NH_3)_3Zn^{II}(HCO_3^-)\cdot H_2O$	−34.0	−28.2
forward Lipscomb	19.1	17.0
backward Lipscomb	25.6	17.7

basically to the formation of two hydrogen bonds. The most striking fact is the important reduction of the two energy barriers. In particular, the barrier for the forward reaction is now 19.1 kcal/mol; i.e., it has decreased by 23.7 kcal/mol when an additional water has been considered for proton release. Likewise, the backward energy barrier is now 25.6 kcal/mol, having been reduced by 28.5 kcal/mol. Inclusion of additional water molecules in the proton release process should affect only very slightly the values for these barriers, as one can expect from the results found by Lipscomb et al.[23,25] using the PRDDO method. These results show that the barrier for the proton transfer in the isolated HCO_3^- anion changes only from 3.5 to 1.4 kcal/mol when two water molecules instead of one water molecule intervene in the proton relay. At the MP2 level, and referred to SCF results, the relative energy of the intermediate hardly changes. This fact differs clearly from the result presented in Table II for the intermediate, although it must be remarked that whereas in Table II the energies are referred to the reactants $(NH_3)_3Zn^{II}(OH^-) + CO_2$, in Table III the point of reference is the energy of the $(NH_3)_3Zn^{II}(OH^-)\cdot CO_2$ complex and an infinitely separated water molecule. The main result is that the forward and backward energy barriers for the Lipscomb mechanism with an additional water molecule become 17.0 and 17.7 kcal/mol, respectively. These values are closer to those presented above for the Lindskog mechanism at the same level of calculation.

(b) Surrounding Medium Effects. So far, we have only considered one additional water molecule in the description of the active site for the Lipscomb mechanism. Actually, the active site contains a number of water molecules and proteinic residues which have not been taken into account yet. This environment is of utmost importance in the study of step 4 of the CA catalytic cycle, where the HCO_3^- anion is exchanged by an incoming water molecule. Surrounding medium effects must stabilize especially the ionic species $(NH_3)_3Zn^{II}(H_2O)$ and HCO_3^-; otherwise it would not be possible to understand how a species with charge (+1) can release two products of charges (+2) and (−1). One can expect that surrounding medium effects may also affect the CO_2 hydration.

Table IV. Solvation Free Energies (ΔG_{solv}) and Their Components (ΔG_{elec} and G_{cav}) for All the Stationary Points Found in the Study of the Lipscomb Mechanism When an Additional Water Molecule Has Been Considered[a]

	$\epsilon = 1.88$			$\epsilon = 78.36$		
	ΔG_{el}	G_{cav}	ΔG_{solv}	ΔG_{el}	G_{cav}	ΔG_{solv}
$(NH_3)_3Zn^{II}(OH^-)\cdot CO_2 + H_2O$	−35.5	14.7	−21.8	−82.2	23.7	−58.5
$(NH_3)_3Zn^{II}(OH^-)\cdot CO_2\cdot H_2O$ INT	−32.4	12.1	−20.3	−72.5	20.2	−52.3
$(NH_3)_3Zn^{II}(OH^-)\cdot CO_2\cdot H_2O$ TS	−35.1	12.1	−23.0	−78.8	20.2	−58.7
$(NH_3)_3Zn^{II}(HCO_3^-)\cdot H_2O$	−29.6	12.6	−17.0	−65.5	21.0	−44.5

[a] All these values have been obtained with the 3-21G basis set, in different two environments of $\epsilon = 1.88$ and 78.36. Energies are given in kcal/mol.

The theoretical modeling of environmental effects in enzymatic processes remains an open question. There are two possible ways to represent the proteinic environment: first, to represent it in a discrete way[79] and, second, to represent it in an average way by means of a continuum model.[80-83] The presence of polar groups in the proteinic chains creates an important electric field which may have an important influence on the reaction. In the present case, water molecules having a restricted motion due to the formation of hydrogen bonds will also contribute to the permanent electric field. The electronic distribution of the chemical system, which changes along the process, will produce an electronic polarization of the environment. Likewise, there is some amount of environment polarization owing to its own reorientation. In turn, the electric field of the environment will electronically polarize the chemical system which will reorientate itself in front of the electric field created by the environment. Therefore, there are at the same time an electronic coupling between the chemical system and the environment and also a certain amount of dynamic coupling through mutual reorientation.

The simplest model in a discrete representation considers the environment by a number of fixed point charges.[79] A first drawback of this model is that electronic polarization of the environment is not included, though this limitation has been overcome by some authors through inclusion of atomic polarizabilities.[84-87] Another drawback of this model is the freezing of the rigid structure of the initial charge distribution. Modern molecular dynamics studies in proteins[88] have shown the inadequacy of this hypothesis. For this reason, more recent models try to account for the coupling between the chemical system and the environment dynamics. The most simple way to study this coupling is the use of a continuum model, where the orientation and intensity of the reaction field depend on the charge distribution in the chemical system at each point of the reaction coordinate. Furthermore, this reaction field produces in turn a polarization of the chemical system. Nevertheless, a continuum model has also strong limitations; for instance, it represents inadequately the permanent electric field created by the environment. For this reason, we should discuss now how to correct this drawback of the continuum model.

A first solution would be to introduce a permanent electric field besides that created by polarization of the dielectric.[89] Nevertheless, we have adopted here another strategy, which consists of taking a large value for the dielectric constant of the environment. Given that reorientation of proteinic residues and water molecules at the active site is partially blocked, it seems that a low dielectric constant to model the environment should be used. However, a proteinic environment differs from a solvent, because in a protein

(79) Tomasi, J.; Alagona, G.; Bonaccorsi, R.; Ghio, C. In *Modelling of Structures and Properties of Molecules*; Horwood, E., Ed.; Ellis Horwood Ltd.: Chichester, England, 1987; p 330.
(80) Krishtalik, L. I.; Topolev, V. V. *Mol. Biol. (Moscow)* **1984**, *18*, 721.
(81) Krishtalik, L. I. *Mol. Biol. (Moscow)* **1974**, *8*, 75.
(82) Krishtalik, L. I. *J. Theor. Biol.* **1985**, *112*, 251.
(83) Krishtalik, L. I. *J. Theor. Biol.* **1980**, *86*, 757.
(84) Melcier, G. A., Jr.; Dijkman, J. P.; Osman, R.; Weinstein, H. In *Quantum Chemistry: Basic Aspects, Actual Trends*; Carbó, R., Ed.; Elsevier: Amsterdam, 1989.
(85) Tapia, O.; Johannin, G. *J. Chem. Phys.* **1981**, *75*, 3624.
(86) Thole, B. T.; van Duijnen, P. T. *Theor. Chim. Acta* **1983**, *63*, 209.
(87) Warshel, A. *Biochemistry* **1981**, *20*, 3167.
(88) McCammon, J. A.; Harvey, S. C. In *Dynamics of Proteins and Nucleic Acids*; Cambridge University Press: Cambridge, 1987.
(89) Warshel, A.; Rusell, S. T.; Sussman, F. *Isr. J. Chem.* **1987**, *27*, 217.

Table V. Charges in Atomic Units on the Atoms or Fragments of the Optimized Intermediate, Transition States, and Product in the Lipscomb Mechanism When an Additional Water Molecule Has Been Considered for the Proton Relay, for Two Different Values of the Dielectric Constant: 1.00 and 78.36[a]

	$q_{(NH_3)_3Zn}$	q_{O_1}	q_{H_1}	q_C	q_{O_2}	q_{O_3}	q_{H_2}	q_{O_4}	q_{H_3}
				ϵ = 1.00					
INT	1.629	−0.903	0.519	1.158	−0.690	−0.769	0.453	−0.817	0.420
TS	1.639	−0.928	0.541	1.188	−0.777	−0.735	0.529	−0.901	0.444
PROD	1.582	−0.833	0.492	1.190	−0.773	−0.743	0.422	−0.762	0.425
				ϵ = 78.36					
INT	1.693	−0.882	0.514	1.162	−0.766	−0.773	0.445	−0.828	0.435
TS	1.703	−0.906	0.554	1.188	−0.845	−0.764	0.518	−0.908	0.460
PROD	1.638	−0.820	0.489	1.175	−0.835	−0.737	0.445	−0.785	0.430

[a] For atom numbering refer to Figure 1.

Table VI. Relative Energies (in kcal/mol) Referred to Separated Reactants for the Different Species Which Intervene in the CO_2 Hydration by CA in the Lipscomb Mechanism When an Additional Water Molecule Has Been Considered in the Proton Release, Together with Forward and Backward Energy Barriers for This Mechanism, Obtained with the 3-21G Basis Set, in Environments of Three Different Dielectric Constants: 1.00, 1.88, and 78.36

	ϵ = 1.00	ϵ = 1.88	ϵ = 78.36
$(NH_3)_3Zn^{II}(OH^-)\cdot CO_2 + H_2O$	0.	0.	0.
$(NH_3)_3Zn^{II}(OH^-)\cdot CO_2\cdot H_2O$ INT	−27.6	−26.1	−21.3
$(NH_3)_3Zn^{II}(OH^-)\cdot CO_2\cdot H_2O$ TS	−8.5	−9.8	−8.6
$(NH_3)_3Zn^{II}(HCO_3^-)\cdot H_2O$	−34.0	−29.2	−20.0
forward energy barrier	19.1	16.3	12.7
backward energy barrier	25.6	19.4	11.4

there is a permanent electric field which has to be taken into account. Therefore, a continuum model like that used in this paper which was developed for solvents must be corrected in some way to account correctly for an enzymatic environmental effect. The use of a large dielectric constant will create a reaction field which accounts much better for the real electric field acting on the chemical system. In this work the study of surrounding medium effects has been performed using two different values of the dielectric constant, one corresponding to an *n*-hexane solution with a low dielectric constant (ϵ = 1.88), and the other corresponding to a water solution with a large dielectric constant (ϵ = 78.36). We think that this latter value represents better the environmental effects in CA.

In Table IV we report the solvation free energies (ΔG_{solv}) and their components (ΔG_{elec} and G_{cav}) for all the stationary points found in the study of the Lipscomb mechanism when an additional discrete water molecule is considered. The most appealing aspect is now the greater stabilization of the transition state referred to the intermediate and product, which carries a decrease of the energy barriers. This stabilization is caused by the large charge separation in this transition state. Comparing the charges presented in Table V for ϵ = 1.00, it can be seen that the charge separation is more important in the transition state than in the reactant intermediate or in the product. Therefore, the stabilization due to the reaction field is stronger in the transition state than in the intermediate or in the product. Another interesting aspect is the polarization of the chemical system. This effect can be seen by comparison of the charges given in Table V for ϵ = 1.00 and ϵ = 78.36. At this point, we should remember that despite having allowed electronic relaxation of the chemical system, its nuclear structure has been kept frozen at the optimized geometries obtained in vacuo. The main effect in this transition state is that, owing to the polarization, the $(NH_3)_3Zn^{II}(OH^-)$ group becomes more positive and the CO_2 fragment more negative. For instance, the CO_2 charge changes from −0.32 to −0.42 when surrounding effects are included, which means that, from an electronic point of view, the nucleophilic attack is now more advanced. Another remarkable fact is that in the transition state the Mayer bond order for the C–O_1 bond increases from 0.713 to 0.797, and the Zn–O_1 decreases from 0.519 to 0.448, which stresses again the fact that the nucleophilic attack is enhanced by the effect of the surrounding medium, even though the geometry of this transition state is kept frozen at the values of the minimum found in the gas phase.

Table VII. Solvation Free Energies (ΔG_{solv}) and Their Components (ΔG_{elec} and G_{cav}) for All the Stationary Points Found in the Study of the Lindskog Mechanism[a]

	ϵ = 1.88			ϵ = 78.36		
	ΔG_{el}	G_{cav}	ΔG_{solv}	ΔG_{el}	G_{cav}	ΔG_{solv}
$(NH_3)_3Zn^{II}(OH^-) + CO_2$	−31.7	14.4	−17.3	−69.0	23.2	−45.8
$(NH_3)_3Zn^{II}(OH^-)\cdot CO_2$ INT	−33.5	11.0	−22.5	−74.7	18.2	−56.5
$(NH_3)_3Zn^{II}(OH^-)\cdot CO_2$ TS	−34.6	11.2	−23.4	−77.2	18.7	−58.5
$(NH_3)_3Zn^{II}(HCO_3^-)$	−33.1	11.3	−21.8	−73.4	18.8	−54.6

[a] All these values have been obtained with the 3-21G basis set, in two different environments of ϵ = 1.88 and 78.36. Energies are given in kcal/mol.

Table VIII. Relative Energies (in kcal/mol) Referred to Separated Reactants for the Different Species Which Intervene in the CO_2 Hydration by CA in the Lindskog Mechanism, Together with Forward and Backward Energy Barriers for This Mechanism, Obtained with the 3-21G Basis Set, in Environments of Three Different Dielectric Constants: 1.00, 1.88, and 78.36

	ϵ = 1.00	ϵ = 1.88	ϵ = 78.36
$(NH_3)_3Zn^{II}(OH^-) + CO_2$	0.	0.	0.
$(NH_3)_3Zn^{II}(OH^-)\cdot CO_2$ INT	−20.3	−25.5	−30.9
$(NH_3)_3Zn^{II}(OH^-)\cdot CO_2$ TS	−18.1	−24.2	−30.7
$(NH_3)_3Zn^{II}(HCO_3^-)$	−31.6	−36.1	−40.4
forward energy barrier	2.2	1.3	0.2
backward energy barrier	13.5	11.9	9.7

Relative energies referred to reactants, and forward and backward energy barriers of the CO_2 hydration for three different values of the dielectric constant (ϵ = 1.00, 1.88, and 78.36), are given in Table VI. Upon examination of these values it can be concluded that the increase of the dielectric constant diminishes the energy barriers and reduces the exothermicity of the reaction. In a dielectric medium of ϵ = 78.36, the decreases of the forward and backward energy barriers are quite important, 6.3 and 14.1, respectively, leading to barriers which are almost identical and favoring the reversibility of the process.

Table VII collects the electrostatic (ΔG_{el}) and cavitation (G_{cav}) contributions to the solvation free energy (ΔG_{solv}) for all species which appear in the study of the Lindskog mechanism when studied through the $(NH_3)_3Zn^{II}(OH^-)$ model. Because of the greater charge separation in the transition state, this structure turns out to be that stabilized most by the environment. However, the difference between the transition state and either the intermediate or the product is not so important as it was in the Lipscomb mechanism. Thus, environmental effects are more significant for the Lipscomb than for the Lindskog mechanism.

Table VIII contains the relative energies referred to separated reactants and the forward and backward energy barriers for the Lindskog mechanism at different values of the dielectric constant. Again it must be remarked that in Tables VI and VIII the energies are referred to different starting points. As in the Lipscomb mechanism, the increase of the dielectric constant implies a decrease of the energy barrier and an increase of the exothermicity of the reaction, though now the effect is less important than in the Lipscomb mechanism. In a surrounding medium of ϵ = 78.36, and referred to in vacuo results, the forward and backward energy

barriers decrease by 2.0 and 3.8 kcal/mol, respectively.

Concluding Remarks

Because of computational limitations we have been unable to introduce the effect of correlation energy and the effect of surrounding medium simultaneously. Nevertheless, we can make the approximation that corrections due to environmental effects and those due to energy correlation at the MP2 level are additive. In this case, the final values for the energy barriers in the Lipscomb mechanism with an additional water molecule turn out to be 10.8 kcal/mol (19.1 - 6.3 - 2.0) for the forward reaction and 3.7 kcal/mol (25.6 - 14.1 - 7.8) for the backward reaction. For the Lindskog mechanism the final value for the forward reaction turns out to be 6.0 kcal/mol (2.2 - 2.0 + 5.8), and for the backward reaction 6.9 kcal/mol (13.5 - 3.8 - 2.8). Thus, both mechanisms are acceptable to explain experimental data, because the values for their energy barriers are close to the maximum allowed value for this CO_2 hydration (ca. 10 kcal/mol).

The model used in the present work, because of computational constraints imposed by the size of the system studied, exhibits obvious limitations such as the level of calculation, the representation of the environment, and the lack of reoptimized geometries when including correlation energy or environmental effects. In any event, the main results of our work are to show that both mechanisms can be competitive in the CA enzymatic process, and that the study of the Lipscomb mechanism needs especially to have a precise modeling of the active site. Therefore, we conclude that, to get a definitive answer on the mechanism of CO_2 hydration catalyzed by the CA enzyme, it is necessary to follow these steps: first, to make a complete description of the active site and, second, to carry out a dynamical study where the coupling between the dynamics of the environment and that of the chemical system is well introduced, which requires that mutual electronic coupling is also well considered. Although this is not possible nowadays, it may be attained in the future.

Acknowledgment. This work has been supported by the Spanish "Dirección General de Investigación Científica y Técnica" under Project No. PB86-0529, and by the Commission of the European Communities (CEE) under Contract SC1.0037.C.

A Potential Surface Map of the H^-/HNO System. Relative Stabilities of NH_2O^- and ^-NHOH

John C. Sheldon* and John H. Bowie

Contribution from the Departments of Chemistry, The University of Adelaide, Adelaide 5001, South Australia, Australia. *Received May 20, 1991*

Abstract: The ion NH_2O^- has been observed in the gas phase, whereas its isomer ^-NHOH has not. The potential surface of the H^-/HNO system has been computed at the UMP2-FC/6-311++G**//RHF/6-31++G* level, and it shows three adducts, i.e. [H^-/HNO] (**1**), NH_2O^- (**2**), and ^-NHOH (**3**). Ion complex **1** is unstable with respect to **2**. Calculations [using the MP4(SDTQ)-FC-6-311++G**//HF/6-31++G** basis set] show that both NH_2O^- and ^-NHOH are strong bases [$\Delta H°_{acid}(NH_2OH)$ = 1629 and $\Delta H°_{acid}(NH_2OH)$ = 1669 kJ mol^{-1}] and that the electron affinities of the radicals $NH_2O^\bullet$ and $^\bullet NHOH$ are −1.2 and −16.7 kJ mol^{-1}, respectively.

Introduction

The nitroxide negative ion NH_2O^- is isoelectronic with the methoxide ion. It has been studied by molecular orbital theory,[1] but has been detected only twice. It may be formed by the reaction between hydroxylamine and HO^- (eq 1),[2] and in small yield by collision-induced dissociation of deprotonated amidoximes (e.g. eq 2).[3] Yet it is an elusive species since it cannot be prepared by the standard S_N2 (Si) reaction[4] from Me_3SiONH_2 (eq 3). Furthermore, its isomer ^-NHOH has not been observed, although it has been proposed that such a species is a powerful base, and that it may be stabilized as part of an ion complex (e.g. eq 4).[5]

$$NH_2OH + HO^- \rightarrow NH_2O^- + H_2O \quad (1)$$

$$Me(NH_2)C{=}NO^- \rightarrow [(MeCN)NH_2O^-] \rightarrow NH_2O^- + MeCN \quad (2)$$

$$NH_2^- + Me_3SiONH_2 \not\rightarrow NH_2O^- + Me_3SiNH_2 \quad (3)$$

$$MeCONOH \rightarrow {}^-CH_2CONHOH \rightarrow [(CH_2CO)^-NHOH] \rightarrow HC_2O^- + NH_2OH \quad (4)$$

We have explored the stability of NH_2O^- and ^-NHOH by the construction of the potential surface of the H^-/HNO system. This paper describes the construction of this surface and its major features. The two $\Delta H°_{acid}$ values of hydroxylamine are also calculated, together with the electron affinities of $NH_2O^\bullet$ and $^\bullet NHOH$.

Results and Discussion

The potential surface map for the reaction between the hydride ion and the HNO molecule is shown in Figure 1; the key features of this map are summarized in schematic form in Figure 2. The map shows three minima corresponding to [H^-(HNO)] (**1**),

(1) Magnussen, E. *Tetrahedron* **1985**, *41*, 5235. Magnussen, E. *J. Am. Chem. Soc.* **1984**, *106*, 1185. Hinde, A. L.; Pross, A.; Radom, L. *J. Comput. Chem.* **1980**, *1*, 118. Dewar, M. J. S.; Rzepa, H. S. *J. Am. Chem. Soc.* **1978**, *100*, 784.

(2) Lifshitz, C.; Ruttink, P. J. A.; Schaftenaar, G.; Terlouw, J. K. *Rapid Commun. Mass Spectrom.* **1987**, *1*, 61. J. K. Terlouw (personal communication) indicates that the ion was formed in the source of a ZAB 2F instrument from a mixture of NH_2OH·HCl, finely powered NaOH, and H_2O in a glass vessel attached to the all quartz direct insertion probe (source pressure 5×10^{-4} Torr). The charge reversal (positive ion) spectrum shows the following relative intensities in the m/z 14–18 region: 14 (10), 15 (20), 16 (100), 17 (13), and 18 (2).

(3) Adams, G. W.; Bowie, J. H.; Hayes, R. N. *J. Chem. Soc., Perkin Trans. 2*, submitted for publication. The ion NH_2O^- is formed in low abundance: its collisional activation spectrum shows loss of $H^\bullet$, but the charge reversal spectrum shows peaks at [m/z (abundance)] 14 (<2), 15 (8), 16 (18), 17 (<2), 30 (100), 31 (25), and 32 (15). The major reaction of ion complex [$(MeCN)NH_2O^-$] (see eq 2) is formation of $^-CH_2CN$ and NH_2OH.

(4) DePuy, C. H.; Bierbaum, V. M.; Flippin, L. M.; Grabowski, J. J.; King, G. K.; Schmitt, R. J. *J. Am. Chem. Soc.* **1979**, *101*, 6443.

(5) Adams, G. W.; Bowie, J. H.; Hayes, R. N. *J. Chem. Soc., Perkin Trans. 2* **1991**, 689. Ion complex [$(CH_2CO)^-NHOH$] (eq 4) does not decompose to yield a detectable ion corresponding to ^-NHOH.

0002-7863/92/1514-877$03.00/0